

Effect of Midpassage Gap, Endwall Misalignment, and Roughness on Endwall Film-Cooling

N. D. Cardwell

N. Sundaram

K. A. Thole

Mechanical Engineering Department,
Virginia Polytechnic Institute and State
University,
Blacksburg, VA 24061

To maintain acceptable turbine airfoil temperatures, film cooling is typically used whereby coolant, extracted from the compressor, is injected through component surfaces. In manufacturing a turbine, the first stage vanes are cast in either single airfoils or double airfoils. As the engine is assembled, these singlets or doublets are placed in a turbine disk in which there are inherent gaps between the airfoils. The turbine is designed to allow outflow of high-pressure coolant rather than hot gas ingestion. Moreover, it is quite possible that the singlets or doublets become misaligned during engine operation. It has also become of interest to the turbine community as to the effect of corrosion and deposition of particles on component heat transfer. This study uses a large-scale turbine vane in which the following two effects are investigated: the effect of a midpassage gap on endwall film cooling and the effect of roughness on endwall film cooling. The results indicate that the midpassage gap was found to have a significant effect on the coolant exiting from the combustor-turbine interface slot. When the gap is misaligned, the results indicate a severe reduction in the film-cooling effectiveness in the case where the pressure side endwall is below the endwall associated with the suction side of the adjacent vane. [DOI: 10.1115/1.2098791]

Introduction

Traditional techniques to cool the hot section of a gas turbine engine involve the use of air from the compressor that has bypassed the combustion chamber and is used for impingement cooling, film cooling, and convective cooling in the turbine airfoils. The coolant is generally high-pressure air that has been routed to the turbine section through a secondary flow path. In the manufacturing of a turbine engine, the airfoils and their associated endwalls are typically cast as singlets or doublets that are then placed in the turbine disk. It is inherently difficult to seal interfaces between the singlets and doublets, particularly when considering the expansion and contraction of turbine components during engine operation. Given that there is high-pressure coolant that must be routed to the turbine through a secondary flow path to cool the blades and vanes, this high-pressure coolant can also leak through any gaps that may exist in the turbine. Moreover, since combustor profiles are not always uniform, it would be expected that the thermal contraction and expansion of adjacent vanes would be significantly different. This difference can lead to turbine airfoils that are misaligned. The question then becomes, how should a turbine designer account for a potential misalignment in airfoil components in their calculations of airfoil temperatures?

Airfoil roughness is an important problem in today's operation of gas turbines. With the push to use fuels other than natural gas, such as coal-derived fuels for industrial turbines, erosion and deposition are issues that must be accounted for. Moreover, propulsive gas turbines are being used in harsh environments in which sand or other foreign debris is ingested and deposited on components in the hot section.

The work presented in this paper compares measured adiabatic effectiveness levels of a well-sealed midpassage gap that is

aligned and misaligned to determine the effect on endwall film cooling and slot cooling. Also compared in this paper is the effect that roughness can have on endwall film cooling.

Relevant Past Studies

There have been turbine endwall studies in the literature that have documented the effects of an upstream slot, discrete film-cooling holes, and combined upstream slot and film cooling. Only a few studies exist on the effect of a midpassage gap. There have been no studies documenting what happens in the case of having a misaligned midpassage gap in an actual airfoil passage. In addition, there have been no studies on the effect of roughness on endwall film cooling.

Most of the studies evaluating leakage flows have been concerned with an upstream slot that represents the leakage flow that might occur between the combustor and turbine. Some of the earliest work related to a leakage flow was performed by Blair [1], who used a two-dimensional aligned slot upstream of vane geometry. Enhancements in film-cooling effectiveness along the endwall were observed as the flow through the slot was increased. In a similar study of coolant upstream of a vane passage, Burd et al. [2] studied the effects of an upstream aligned, 45 deg slot. By using coolant flows as high as 6% of the total passage flow, better cooling was observed over the endwall and on both sides of the vanes relative to lower coolant flows. A study by Colban and Thole [3,4] measured the effects of changing the combustor liner film cooling and upstream slot flows on the effectiveness levels along the endwall of a first-stage turbine vane. Their results showed that the coolant from the slot was not uniform across the exit, with coolant accumulating along the endwall near the suction side of the vane. Coolant injection from the upstream combustor liner caused a different total pressure profile entering the vane passage, relative to a turbulent boundary layer, that in turn changed the secondary flow field.

Detailed endwall film-cooling results have been conducted by Friedrichs et al. [5–7]. The results of their first study [5], which were all surface measurements or visualization, indicated a strong

Contributed by the International Gas Turbine Institute (IGTI) of ASME for publication in the JOURNAL OF TURBOMACHINERY. Manuscript received October 1, 2004; final manuscript received February 1, 2005. IGTI Review Chair: K. C. Hall. Paper presented at the ASME Turbo Expo 2005: Land, Sea, and Air, Reno, NV, June 6–9, 2005, Paper No. GT2005-68900.

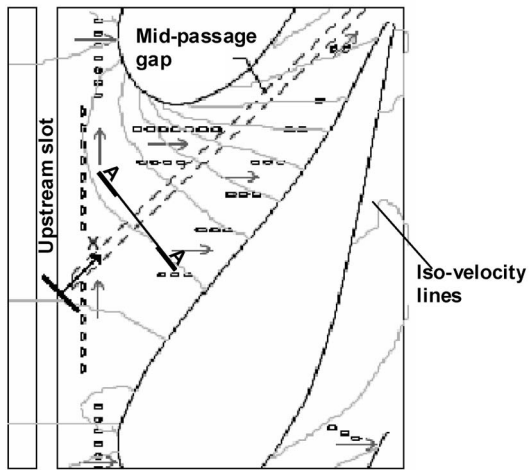


Fig. 1 Directions of the coolant hole injection along with iso-velocity contours and the midpassage gap location for mating two turbine vane platforms

influence of the secondary flows on the film cooling and an influence of the film cooling on the secondary flows. Their data showed that the angle at which the coolant leaves the hole did not dictate the coolant trajectory except near the hole exit. Furthermore, the endwall cross flow was altered so that the cross flow was turned toward the inviscid streamlines, which was due to the film-cooling injection.

The only studies to have combined an upstream slot with film-cooling holes in the passage of the vane were those of Zhang and Jaiswal [8], Kost and Nicklas [9], Nicklas [10], and Knost and Thole [11,12]. One of the most interesting results from the Kost and Nicklas [9] and Nicklas [10] studies was that they found for the slot flow alone, which was 1.3% of the passage mass flow, that the horseshoe vortex became more intense. This increase in intensity resulted in the slot coolant being moved off of the endwall surface and heat transfer coefficients that were over three times that measured for no slot flow injection. They attributed the strengthening of the horseshoe vortex to the fact that for the no slot injection the boundary layer was already separated, with fluid being turned away from the endwall at the injection location. Given that the slot had a normal component of velocity, injection at this location promoted the separation and enhanced the vortex. Their adiabatic effectiveness measurements indicated higher values near the suction side of the vane due to the slot coolant migration. Knost and Thole reported a significant change in the streamlines in the near-endwall region resulting from the upstream slot flow. Their results also indicated that the momentum flux ratio was an important parameter in predicting the cooling jet behavior.

Using a flat plate geometry with no turbine airfoils, Yu and Chyu [13] studied the influence of gap leakage downstream of injection cooling holes. They observed that for a moderate level of film cooling upstream of a coolant slot, the combined presence with the gap promoted better coolant film protection. However, as the film-cooling flow was increased the coolant from the gap appeared to lift the slot flow coolant from the wall, resulting in decreased adiabatic effectiveness.

The only known studies of flow from a slot within the midpassage of adjacent airfoils were performed by Aunapu et al. [14], Ranson and Thole [15], and Yamao et al. [16]. Aunapu et al. used blowing through a passage gap in an attempt to reduce the effects of a passage vortex. They hypothesized endwall blowing in the blade passage could reduce the effects of the passage vortex. Aunapu et al. [14] observed that endwall jets in the center of the blade passage effectively altered the path of the pressure side leg of the vortex. Unfortunately, the increased blowing caused higher turbulence and higher aerodynamic losses. Ranson and Thole used

Table 1 Geometric and flow conditions

Scaling factor	9
Scaled up chord length (C)	59.4 cm
Scaled up axial chord length	29.3 cm
Pitch/chord (P/C)	0.77
Span/chord (S/C)	0.93
Re_{in}	2.1×10^5
Inlet and exit angles	0 & 72 deg
Inlet, exit Mach number	0.017, 0.085
Inlet mainstream velocity	6.3 m/s

an aligned midpassage gap between two adjacent blades for their combined experimental and computational studies. Their results indicated that the flow leaving the gap was directed toward the blade pressure side, as a result of the incoming velocity vector, and then traversed towards the suction side of the adjacent airfoil. Yamao et al. [16] investigated the distribution of film-cooling effectiveness due to sealing air injected from combustor-vane interface and vane-to-vane interface on annular cascade test equipment. Their study indicated that the film-cooling effectiveness was enhanced with an increase in the sealing air flow rate between the vanes. Also, the increase in sealing air flow rate between the combustor-vane interfaces resulted in significant increase in film-cooling effectiveness near the leading edge, but a slight increase along the trailing edge.

In summary, it is important to understand the effect of coolant flow from leakage points in the endwall region under realistic surface conditions to further the technology of turbine blade cooling. To date, there have been only a few studies that have addressed roughness effects on an actual turbine airfoil but none of these studies has addressed the effect of roughness with adiabatic effectiveness levels on a film-cooled endwall.

Midpassage Gap Geometry

The flat endwall in the linear cascade used for these studies was comprised of five realistic features: a combustor to turbine (upstream) gap, endwall film cooling, a midpassage gap with accompanying strip seal, the capability of simulating an endwall misalignment, and surface roughness representative of that found in an engine. The first-stage vane endwall film-cooling pattern, which was originally designed and tested by Knost and Thole [12], is shown in Fig. 1, which also shows iso-velocity contours and hole injection angles. All film-cooling holes were at an angle of 30 deg with respect to the endwall surface.

Also included in the endwall pattern is a two-dimensional slot representing the interface between the combustor and first stage of the turbine. This slot is located 30% of the axial chord upstream of the vane stagnation location, and is designed to be forward facing with an injection angle of 45 deg with respect to the endwall surface. This leakage interface will be referred to as the upstream slot. Table 1 provides a description of turbine vane geometry and

Table 2 Summary of endwall geometry

	Parameter	Experimental
Midpassage gap	W -Passage gap width	0.01C
	H -Seal strip thickness	0.5W
	A -Thermocouple location	6H
	B -Passage gap depth	10H
	C -Seal strip gap	2H
	D -Seal strip width	16.8H
	E -Passage gap plenum width	28H
Upstream slot	Upstream slot width	0.024C
	Slot flow length to width	1.88
Film cooling	FC hole diameter (cm)	0.46
	FC Hole L/D	8.3

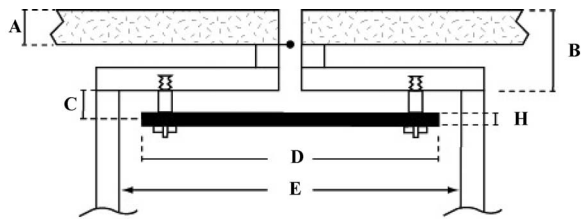


Fig. 2 Cross-section view (section AA, Fig. 1) of the midpassage gap plenum and accompanying seal strip (see Table 2)

operating conditions, and Table 2 provides a summary of parameters relevant to film cooling and upstream slot geometries.

The focus of this paper, as explained, is the interface between the combustor and turbine flows. Also, the midpassage gap does not open into the upstream slot and has its own supply plenum. The dimensions and arrangement of the midpassage gap plenum are shown in Table 2 and Fig. 2. The vane-to-vane interface has three distinct alignment modes: aligned, forward-facing step (dam), and backward-facing step (cascade). The aligned mode, which is shown in Fig. 3(a), represents no disparity in height between adjacent vanes and the combustor.

The offset that was considered for the misaligned endwall was 1.2% of vane height or 0.65 cm for the $9\times$ scale geometry. The dam endwall refers to a condition where the suction surface of vane 1 (V1) is raised relative to the pressure side of vane 2 (V2), which is flush with the combustor wall. This configuration is referred to as a dam because, as the secondary flows are driven from the pressure side of one vane towards the suction side of the adjacent vane, the flow faces an upward step. Figure 3(b) shows the dam configuration has a raised step for V1 at the upstream slot location.

The cascade endwall refers to a condition where the suction surface of V1 is lowered relative to the pressure side of V2, which is flush with the combustor wall, as shown in Fig. 3(c). This configuration is referred to as a cascade because the secondary flows from the pressure to the suction side experience a waterfall, or cascade, effect. For the cascade case, the upstream slot has a recessed step for the vane 1 portion of the platform.

Relative to the work that was done by Knost and Thole [12], endwall roughness was also investigated. For this simulation, the study completed by Bons et al. [17] was referenced to model realistic surface roughness on a first-stage vane platform. Bons et al. lists measured values of endwall rms roughness height (R_a) as $28\ \mu\text{m}$. This rms value translates to an equivalent sand grain roughness (k_s) of 196 microns as described by Bogard et al. [18]. At $9\times$ scale, which is the scaling factor for the test vane, it resulted in equivalent sand grain roughness (k_s) of 1.76 mm.

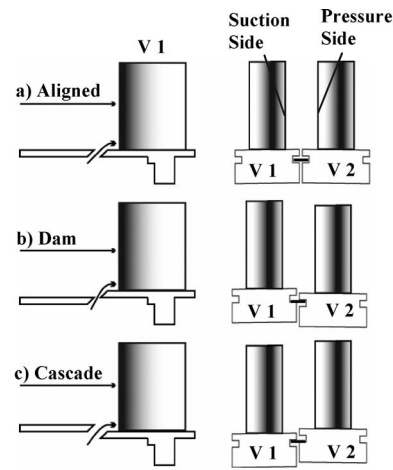


Fig. 3 Side and upstream views of the three alignment modes for two adjacent vane platforms

To simulate a uniformly rough surface, wide-belt industrial sandpaper was used to cover the entire endwall. It has a closed-coat 36-grit surface and grade Y cloth backing. The 36-grit sandpaper corresponds to an equivalent sand grain roughness of 418 microns at engine scale (www.sizes.com/tools/sandpaper.htm). A closed-coat surface has roughness elements arranged in a random array over 100% of the surface. Custom construction of the sandpaper was used to guarantee tight tolerances around each film-cooling hole. This ensured that the rough surface does not block the hole, and that the interaction between the rough surface and coolant jets is uniform for the entire endwall.

Experimental Methodology

The experimental facility included a test section placed in a wind tunnel, as shown in Fig. 4. The test section consisted of a vane scaled up by a factor of 9 with cooling holes and slot geometries. Adiabatic endwall temperature measurements were taken for different flow rates through film-cooling holes and through the slot representing the combustor turbine interface. For the present study, there was no flow through the midpassage gap at the interface of the vanes. This was primarily done to study the aerodynamic effect caused by the presence of the gap, and to simulate a perfectly sealed interface.

The test section was placed inside the closed-loop wind tunnel facility shown in Fig. 4, a detailed account of its construction has been previously described by Knost and Thole [12]. The difference in this test section from the one used by Knost and Thole is the presence of a rough endwall surface and the presence of a

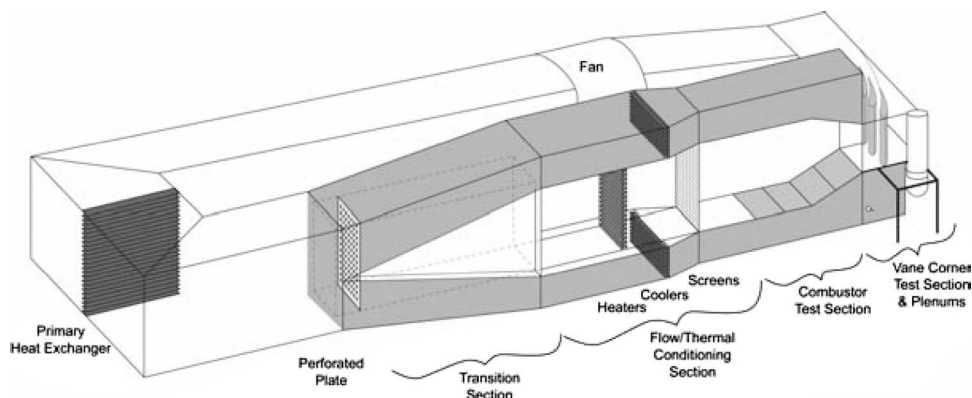


Fig. 4 Illustration of the wind tunnel facility

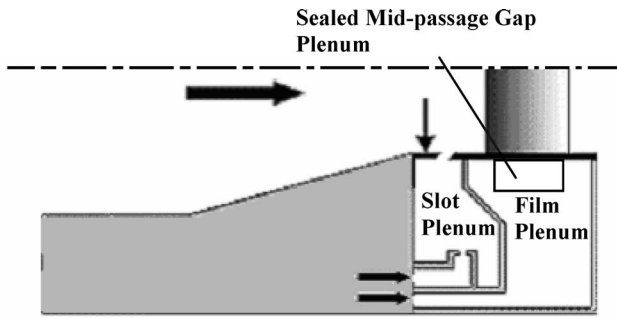


Fig. 5 Separate plenums for film cooling and upstream slot provided independent control of the flow through each of them

midpassage gap between the endwalls of the adjacent vanes. The flow in the wind tunnel is driven by a 50 hp axial vane fan, which is controlled by a variable frequency inverter. Downstream of the fan, the flow encounters a 90 deg turn and passes through a primary finned-tube heat exchanger used to cool the bulk flow. After the heat exchanger, the flow encounters a three-way flow split. Note that only the bottom channel was used for this study. This split was done to create a primary core flow and a cooled secondary flow. The primary core flow was made to pass through a heater bank consisting of three heaters where the air temperature was increased to 55°C. The secondary flow, in the outer channel, was made to pass through a secondary heat exchanger where the flow temperature was lowered to about 15°C. The secondary flow path represented the coolant flow through the film-cooling holes and the slots.

The test section consisted of two full passages with one center vane and two half vanes. It is important to note that film-cooling effectiveness studies were done only in the passage where the midpassage gap was simulated. The test section consisted of separate plenums for independent control of flow through the film-cooling holes and the upstream slot, as shown in Fig. 5. A temperature difference of about 40°C was maintained at all times between the mainstream and coolant flows under steady-state conditions.

Typical times to achieve steady state conditions were 3 h. The free-stream turbulence effects were not taken into consideration, as these studies were more focused on industrial gas turbines rather than on aero engines. Free-stream turbulence levels are generally higher for aero engines when compared to industrial gas turbines. The inlet turbulence effects and length scales were measured to be 1.3% and 4 cm, respectively. The endwall of the vane, which was the main focus of study, was constructed of foam because of its low thermal conductivity (0.033 W/m K). The end-wall foam was 1.9 cm thick and was mounted on a 1.2 cm thick Lexan plate. The cooling hole pattern on the endwall was cut with a five-axis water jet to ensure precision and integrity. The upstream slot was constructed with hard wood, as it had a low conductivity and was stiffer.

Coolant Flow Settings. For every test condition the dimensionless pressure coefficient distribution was verified to ensure periodic flow through the passages. As stated earlier, two separate plenums were used to control the flow rate through the film-cooling holes and through the upstream slot. Friedrichs et al. [5] suggested that a global blowing ratio based on the inlet flow conditions could be characterized by the blowing ratio of a loss-free hole injecting into inlet conditions calculated from

$$M_{\text{ideal}} = \sqrt{\frac{\rho_c P_{o,c} - P_{s,\text{in}}}{\rho_{\text{in}} P_{o,\text{in}} - P_{s,\text{in}}}} \quad (1)$$

A modification of this approach was done in this study, and a global discharge coefficient, C_D , was derived so that a cumulative

Table 3 Summary of Coolant Settings

% Mass flow	C_D	M_{ideal}	M_{actual}
0.35 Film cooling	0.85	1.24	1.06
0.50 Film cooling	0.8	1.88	1.51
0.75 Film cooling	0.71	3.2	2.26
0.75 Upstream slot	0.6	0.48	0.29
0.95 Upstream slot	0.6	0.69	0.414
1.10 Upstream slot	0.6	0.72	0.43

flow rate through the film-cooling holes could be defined. These C_D values were obtained from computational fluid dynamics (CFD) studies done on a similar geometry, and were reported earlier by Knost and Thole [11]. Measurements of the inlet velocity, average inlet static pressure, and coolant total pressures were obtained which then allowed the fraction of coolant flow relative to the inlet core flow to be calculated from

$$\frac{\dot{m}_c}{\dot{m}_{\text{core}}} = M_{\text{ideal}} \cdot C_D \cdot \frac{A_{\text{hole}}}{A_{\text{in}}} \cdot \# \text{ holes} \quad (2)$$

The upstream slot flow was assumed to have a discharge coefficient of 0.6, which is the assumed value for a flow through a sharp-edged orifice, and the flow rate was calculated accordingly. Table 3 gives a description of the actual and ideal global blowing ratios used for the different film-cooling and upstream slot mass flow rate settings.

Instrumentation and Temperature Measurements. An FLIR P20 infrared (IR) camera was used to capture the spatially resolved adiabatic wall temperatures on the endwall. Measurements were taken at seven different viewing locations to ensure that the entire endwall surface was mapped. The camera was placed perpendicular to the endwall surface at a distance of 55 cm. Each picture covers an area 24 by 18 cm, with the area being divided into 320 by 240 pixel locations. The spatial integration of the camera was 0.715 mm (0.16 hole diameters). Thermocouples were also placed on the endwall surface at different locations to directly measure the temperature to postcalibrate the infrared images. For the postcalibration the emissivity and background temperature were adjusted until the temperatures from the infrared camera images were within 1°C of the corresponding thermocouple data. Typical emissivity values and background temperatures were 0.92 and 45°C (note that the free-stream temperature was 55°C). Five images were taken at each of the viewing locations to obtain an averaged picture using an in-house MATLAB program. The same program was also used to assemble the averaged pictures at all locations to give a complete temperature distribution along the passage endwall.

Free-stream temperatures were measured at multiple locations along the pitch, and the average was determined by using a thermocouple rake consisting of three thermocouples along the span. It was found that the variations along the pitch were less than 0.2°C and those along the span were less than 1.5°C. Three thermocouples were attached in the upstream slot location at the combustor exit, and two thermocouples were attached in the film-cooling plenum. Eleven thermocouples were placed in the midpassage gap to measure the temperature profile along the gap. The thermocouples in the midpassage gap were placed 6 seal strip thicknesses beneath the surface, which was roughly one-third of the slot flow length beneath the surface (Table 2). Voltage outputs from the thermocouples were acquired by a 32-channel data acquisition module that was used with a 12-bit digitizing card. The temperature data were compiled after the system reached steady state.

An uncertainty analysis was performed on the measurements of adiabatic effectiveness using the partial derivative method described at length by Moffat [19]. The precision uncertainty was determined by taking the standard deviation of six measurement

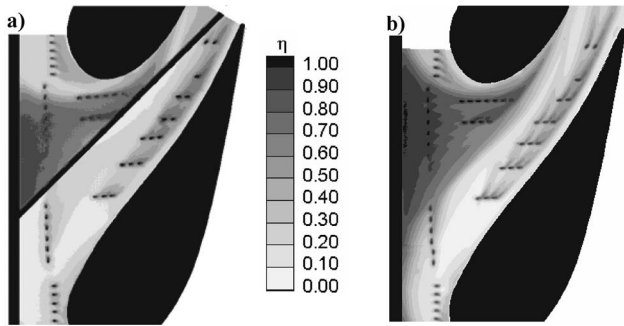


Fig. 6 Contours of adiabatic effectiveness for film-cooling cases (a) rough endwall with midpassage slot and (b) smooth endwall with no midpassage slot

sets of IR camera images, with each set consisting of five images. The precision uncertainty of the measurements was $\pm 0.014^\circ\text{C}$. The bias uncertainty was $\pm 1.0^\circ\text{C}$ based on the calibration of the image. The bias uncertainty of the thermocouples was $\pm 0.5^\circ\text{C}$. The total uncertainty was then calculated as $\pm 1.0^\circ\text{C}$ for the images and $\pm 0.51^\circ\text{C}$ for the thermocouples. Uncertainty in effectiveness, η , was found based on the partial derivative of η with respect to each temperature in the definition and the total uncertainty in the measurements. Uncertainties of $\partial\eta = \pm 0.082$ at $\eta = 0.2$ and $\partial\eta = \pm 0.029$ at $\eta = 0.9$ were calculated. A one-dimensional conduction analysis was performed at the entry and exit of the passage to calculate the conduction error. The resulting η correction was found to be 0.07 at the entrance and 0.02 at the exit region at a measured η value of 0.5.

Discussion of Results

As stated previously, all tests and data acquisition were completed for no flow through the midpassage gap. First, the effect of the presence of the midpassage gap and roughness will be discussed for an aligned endwall. The results from this test will be compared with an existing case having no midpassage gap. Second, a comparison of results obtained for aligned and misaligned midpassage gap will be discussed.

Film-Cooling Effectiveness With a Rough Endwall and a Midpassage Gap. The nominal film-cooling cases with and without a midpassage slot for 0.75% upstream slot flow and 0.5% film-cooling flow are shown in Figs. 6(a) and 6(b). Note that the percentages refer to the coolant flow relative to the hot gas path flow. There are two noticeable effects that can be determined by comparing these two cases that include the effect of the midpassage gap and the effect of roughness.

It can be seen from Fig. 6(a) that there is no coolant flow from the upstream slot crossing over the midpassage gap location. This condition becomes apparent when comparing the contours of Fig. 6(a) with those of Fig. 6(b) where, in the absence of the gap, the coolant from the upstream slot convects towards the suction side of the vane sweeping over a large area of the endwall. In the presence of the midpassage gap, Fig. 6(a) shows no coolant exiting the upstream slot on the pressure side of the midpassage gap. The reason for this lack of coolant is that the coolant from the upstream slot is ingested until the end of the vane passage where it then exits the gap. This effect will be discussed further in a later section of the paper. As a result of this degradation of the coolant on the pressure side of the midpassage gap, the hot streak through the center of the passage appears to be wider with the presence of a midpassage gap relative to the no-gap case. In determining the effect of roughness on the endwall film cooling, comparisons can also be made between Figs. 6(a) and 6(b).

Observing the coolant exiting from the leading edge holes upstream of the stagnation location on the suction side, one can see

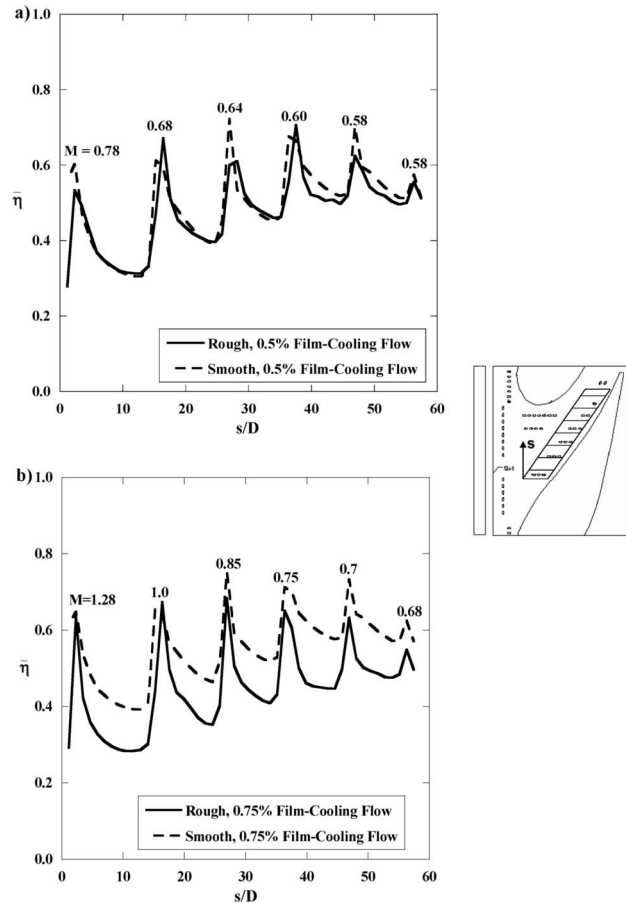


Fig. 7 Plots of laterally averaged adiabatic effectiveness on the film-cooling holes on the pressure side: (a) for 0.75% upstream slot flow and 0.5% film cooling and (b) 0.75% upstream slot flow and 0.75% film cooling

that the coolant is dispersed more rapidly for the case with the rough endwall relative to the smooth endwall. Along the pressure side, the jets merge more evenly in the case of the rough endwall relative to the smooth endwall, where in the case of the smooth endwall there are distinct jets.

To quantify the effects of roughness, a section of the endwall near the pressure side of the vane, as shown in Fig. 7, was further analyzed. Figures 7(a) and 7(b) show the effect of roughness on the laterally averaged effectiveness for 0.5% and 0.75% film-cooling flows, respectively. Also indicated in Fig. 7 are the row-averaged local blowing ratios for each row of holes along the pressure side. Note that CFD results were used to quantify the local coolant flows from each cooling hole, and the local static pressure was used to calculate the local free-stream velocity that was used in the blowing ratio definition. For the 0.5% case, where the local blowing ratios ranged from 0.58 to 0.78, the laterally averaged effectiveness values indicate that there is essentially no effect of roughness of the film-cooling performance. In looking at the contours in Figs. 6(a) and 6(b), however, there are some local differences indicated particularly with the jet merging.

For the higher coolant flow condition in Fig. 7(b), where the local blowing ratio ranges from 0.68 to 1.28, there is a dramatic decrease in the average effectiveness along the pressure side with roughness. The decrease in the laterally averaged effectiveness due to roughness is on the order of 30% midway between film-cooling rows. One plausible reason for the larger decrease at the higher blowing ratio relative to the lower blowing ratio is because for a rough wall the boundary layer is thicker, thereby allowing the jets to separate from the endwall. As the front jet separates

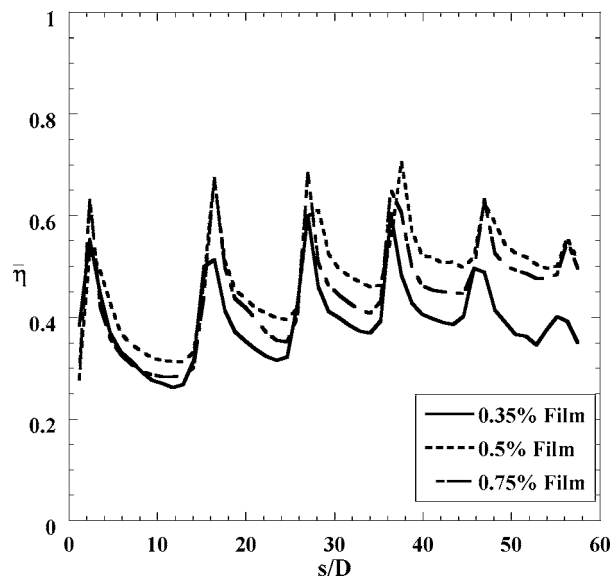


Fig. 8 Laterally averaged adiabatic effectiveness for 0.35%, 0.5%, and 0.75% film-cooling flows for a rough endwall

from the wall, this effect is compounded as one progresses downstream along the pressure side. This reduction in film-cooling effectiveness may also be attributed to increased interaction with hot mainstream. The rough surface greatly increases boundary layer thickness and turbulence levels, causing enhanced mixing between the coolant and mainstream and thereby lowering area-averaged values of adiabatic effectiveness.

In comparing Fig. 7(a) and Fig. 7(b), it is seen that there is a benefit in cooling when increasing the coolant flow from 0.5% to 0.75% for the smooth wall case. In contrast, when increasing the coolant flow for the rough wall case, the average adiabatic effectiveness levels actually decrease with an increase in blowing ratio. As such, Fig. 8 compares the laterally averaged effectiveness values for the rough endwall case along the pressure side holes for three different coolant flow rates: 0.35%, 0.5%, and 0.75%. The corresponding contours for these lateral averages just along the pressure side are shown in Figs. 9(a)–9(c). As is typically expected, by increasing the film-cooling flow from 0.35% to 0.5%, one sees that there is an increased gas performance in the film-cooling effectiveness levels. In comparing the contours shown in Figs. 9(a) and 9(b), it is clear that the first row of holes in the averaging area defined in Fig. 7 appears nearly the same between the two cases, but that cooling appears to be much better at the second row for the higher blowing ratio case.

By increasing the coolant flow to 0.75%, the laterally averaged effectiveness significantly decreases relative to the 0.5% coolant flow case but is better than the 0.35% coolant flow case, as shown in Fig. 8. The contours in Fig. 9(c) indicate better penetration towards the pressure side of the endwall for the 0.75% coolant flow case, but that the overall levels of effectiveness downstream of the film-cooling holes are significantly lower than for the 0.5% coolant flow case. These contours indicate that, as the jets penetrate closer to the pressure side surface, they are also lifted off the surface. Knost and Thole [11] observed a similar trend for the smooth wall case in that the pressure side film-cooling jets appeared to be lifted off the surface for the 0.75% coolant flow case, but as seen from Fig. 7(b) this effect is worsened with roughness.

Outside of the averaging area, at the most upstream row of film-cooling holes, the contours in Figs. 9(a)–9(c) indicate little change in effectiveness levels as a function of increased coolant levels. There was only slightly better performance for the 0.5% coolant flow condition relative to the 0.35% and 0.75% coolant flows. Just upstream of the stagnation location, the contours in

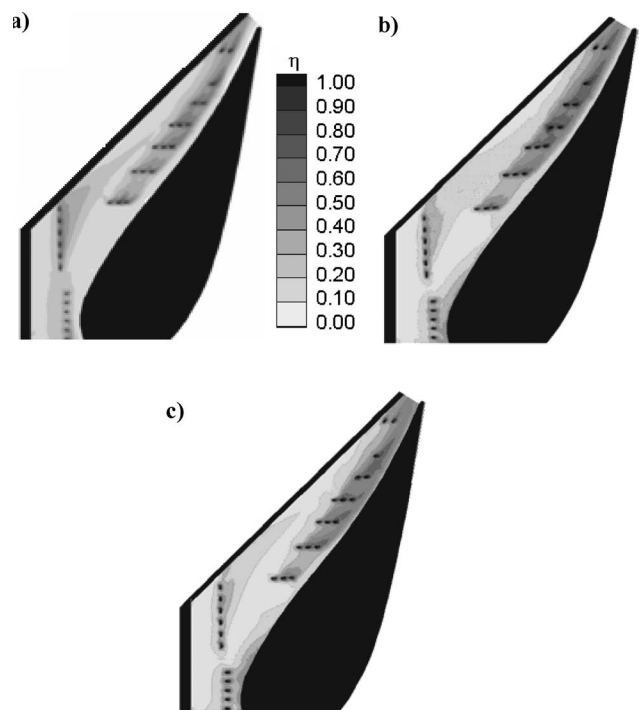


Fig. 9 Contours of adiabatic effectiveness with a rough endwall with 0.75% slot flow for (a) 0.35% film cooling; (b) 0.5% film cooling; (c) 0.75% film cooling

Figs. 9(a)–9(c) indicate that, for the 0.5% and 0.75% coolant flow conditions, the leading-edge film-cooling jets are impacting the vane and then being washed back down onto the surface, indicating some coolant at the vane-endwall junction.

Effect of a Misaligned Midpassage Gap. One of the primary questions raised for this work was how to best design an endwall simulating the surface roughness and turbine vane misalignment. As was discussed previously, there is a possibility for an aligned endwall configuration, a cascade endwall configuration, and a dam endwall configuration. The misalignment value was set to 1.2% of the vane span. For these comparisons, both the film-cooling and upstream slot flows remained constant at 0.5% and 0.75% of the core flow, respectively. Figures 10(a)–10(c) correspond to aligned, dam, and cascade endwall configurations, respectively. Indicated on these figures is the portion of the endwall that is raised (U) and lowered (D). For explanatory purposes, the section of endwall closest to the top vane picture is referred to as the suction side section, and the section of the endwall closest to the bottom vane will be referred to as the pressure side section.

In comparing the aligned case to the dam case, it can be seen that in the case of the dam the overall platform cooling is much worse than in the case of the aligned endwall. It appears that, because of the front slot misalignment, the leakage coolant from the upstream slot is directed into the hot gas path rather than along the endwall. It is also interesting to look at the end of the midpassage gap. Figure 10(a) for the aligned endwall indicates that at the midpassage gap exit, coolant exits the slot. This coolant was the upstream slot coolant and film coolant that was ingested into the slot and then exited at the lowest external static pressure location. In the case of the dam endwall, Fig. 10(b) indicates that there is no coolant exiting the end of the midpassage slot. It is also quite interesting to see the diminished effectiveness levels in the vicinity of the midpassage slot at about 20% of the slot length measured from the upstream slot shown in Fig. 10(b). This warmer region was also shown for aligned endwall in Fig. 10(a), but it is

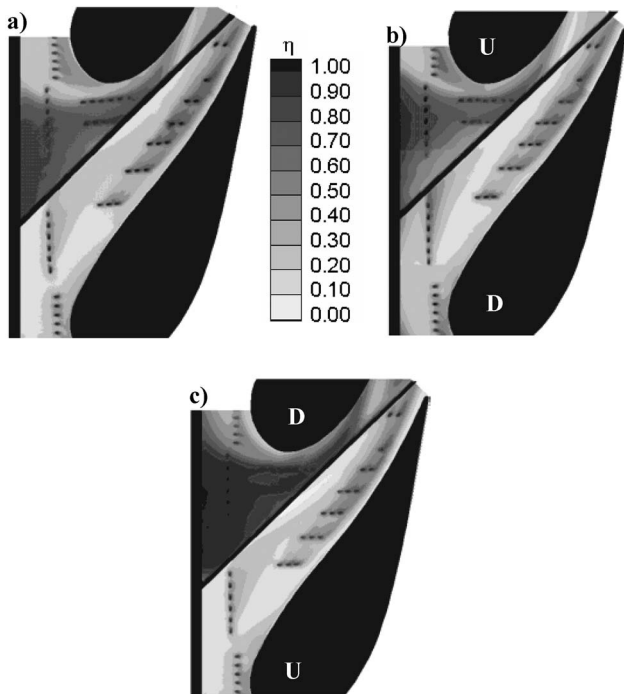


Fig. 10 Contours of adiabatic effectiveness on a rough endwall for the baseline film and slot cooling cases: (a) aligned, (b) dam, and (c) cascade endwall (note that *U* refers to raised side and *D* refers to lowered side)

not as dramatic. At this location, there is no upstream slot flow present, which was worsened for the dam configuration, nor is there any film-cooling flow present.

When the endwall surface is set to cascade configuration, coolant from the upstream slot can flow in an unobstructed manner onto the endwall. The effectiveness contours in Fig. 10(c) indicate a much improved performance for the cascade case relative to both the aligned and the dam configurations. The lowered endwall in the case of the cascade acts like a trough in which the upstream slot flow does not mix out as quickly with the mainstream hot gas. As a result, higher effectiveness values occur on the suction side portion of the endwall. For the cascade configuration, the pressure side contours are very similar to the aligned endwall configuration, because there is no blockage for the secondary flows, as compared with the dam case. At 20% slot length downstream from the upstream slot the warm region previously discussed is diminished for the cascade condition relative to both the dam and aligned cases.

Figure 11(a) compares the pitchwise-averaged effectiveness along the suction side of the endwall for the three endwall configurations, and Fig. 11(b) compares the effectiveness distribution along the suction and pressure sides for the aligned case. Figure 11(a) clearly substantiates the previous results that the cascade configuration results in better cooling along the suction side, and Fig. 11(b) strengthens the conclusion that there is better cooling on the suction side than on the pressure side for any kind of endwall configuration. It was also found that the pitchwise-averaged effectiveness on the pressure side for the three endwall settings remained the same. The area-averaged effectiveness was higher for the cascade configuration when compared to the aligned or dam. The area-averaged effectiveness levels, which include both the pressure and suction side portions of the endwall, were 0.49 for cascade, 0.45 for the aligned, and 0.42 for the dam, respectively.

As was previously discussed, the air temperature inside the gap was measured as indicated in Fig. 2. Recall that for the study reported in this paper there was no flow exiting the midpassage

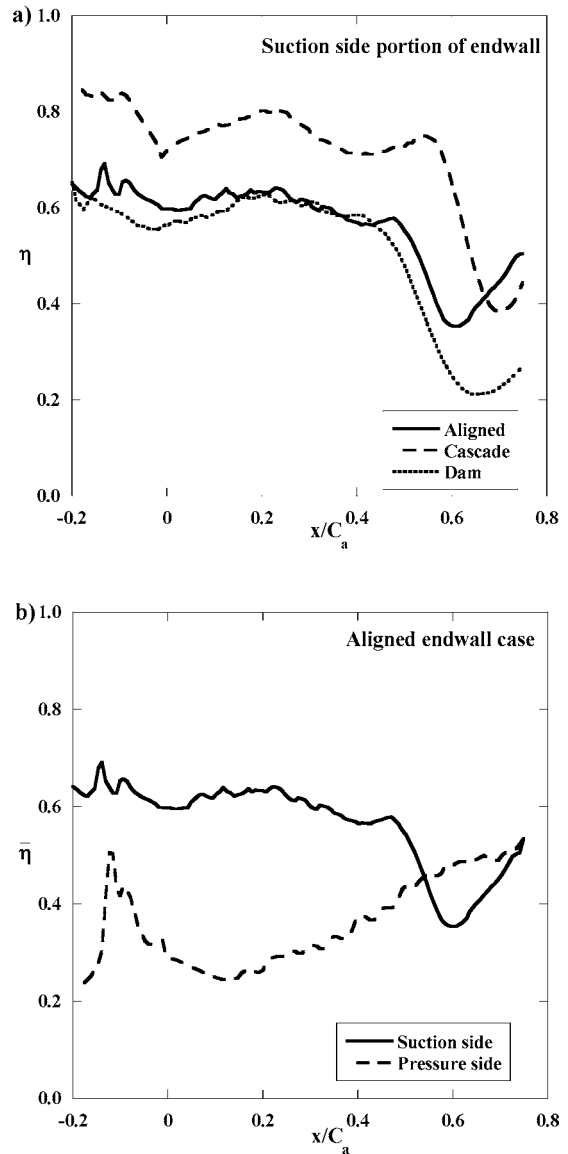


Fig. 11 Pitchwise-averaged adiabatic effectiveness for the baseline film and slot cooling cases: (a) along the suction side for the three endwall settings; (b) comparison between effectiveness on the suction and pressure side

gap such that the temperatures measured were those of any flow that might ingest into the midpassage slot. The measured nondimensional gap temperatures for the aligned and misaligned cases are shown in Fig. 12. The nondimensionalization was based on the coolant temperature and hot gas free-stream temperatures. Also shown in Fig. 12 are the inviscid gap velocities that were calculated based on the local static pressure at the gap exit. Note that this inviscid analysis assumed a constant total pressure difference between the mainstream and the gap plenum. An iterative procedure was used to calculate the pressure difference which resulted in zero net mass flow from the slot (ingested flow balanced with exiting flow).

Figure 12 shows that, for the aligned and dam cases, a large amount of coolant is ingested into the leading edge of the midpassage gap region relative to the cascade case. In the location $0 < x/L < 0.2$ there is coolant ingestion from the upstream slot resulting in higher θ , with the amount of coolant being ingested decreasing with an increase in x/L . There is also increased ingestion of the mainstream flow, causing a rapid rise in the gap air

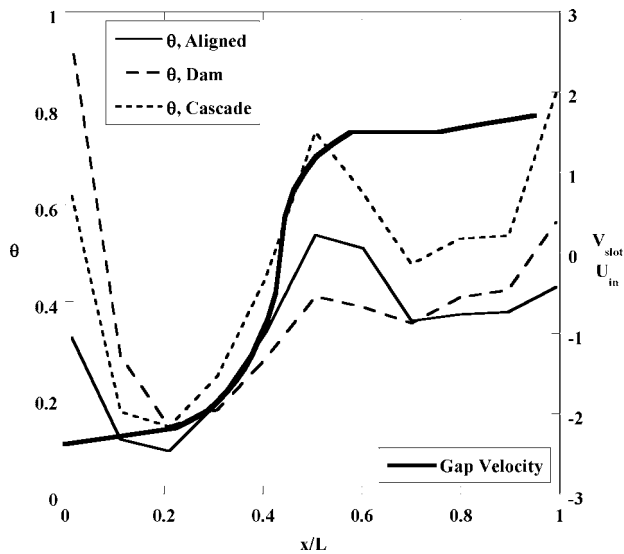


Fig. 12 Nondimensionalized gap temperature profiles for the three endwall alignment modes and the velocity profile for an aligned gap

temperature and hence a decrease in θ . The nondimensional temperatures in the gap decrease dramatically as hot mainstream flow is ingested near $x/L=0.2$. For the midpassage gap location between $0.3 < x/L < 0.5$, all of the endwall cases show a decrease in the air temperature (increase in θ) along the midpassage gap, which results from a fresh influx of coolant from the two rows of film-cooling holes directly upstream of this region (see Figs. 10(a)–10(c)). The dam case benefits less because of the step, in conjunction with the cross-passage secondary flows that forces more hot flow into the gap. Figure 12 also shows that the temperatures inside the gap associated with the cascade endwall setting are cooler than that for the dam endwall setting, which is because of the cooler fluid from the upstream slot. Up to $x/L=0.5$, the inviscid velocity is indicated to be into the slot (static endwall pressure is higher than the plenum pressure), which is consistent with the fact that flow is ingesting into the slot.

Beyond $x/L=0.5$, Fig. 12 shows that flow exits the midpassage gap. Between $0.5 < x/L < 0.7$, there is an increase in the temperature within the midpassage gap, which is followed by a decrease beyond $x/L=0.9$. The slight increase at the exit results from any coolant that was channeled through the midpassage gap from the upstream slot.

Effect of Slot Flow with a Cascade Endwall. Because the best configuration appeared to be the cascade endwall, more studies were completed with this configuration whereby flow from the upstream slot was varied. As previously discussed, the coolant flow from upstream slot has little effect on the pressure side of the midpassage slot. Figure 13 compares adiabatic effectiveness contours for different slot flow rates (or different momentum flux ratios) with cascade endwall setting. The momentum flux ratios were calculated for all the flow rates through the slot using the relation

$$I = \frac{\rho_s u_s^2}{\rho_\infty U_\infty^2} = \frac{\rho_s (m/\rho_s A_s)^2}{\rho_\infty U_\infty^2} \quad (3)$$

It can be seen in Fig. 13(a), that, for 0.75% slot flow, there is little cooling around the leading edge holes on the pressure side. With an increase in the slot flow rate, however, the adiabatic effectiveness near the upstream slot region increases, indicating some coolant exiting from the upstream slot onto the pressure side of the midpassage gap as seen in Fig. 13(b) and Fig. 13(c). It is also interesting that, as the upstream slot flow is increased, the warmer

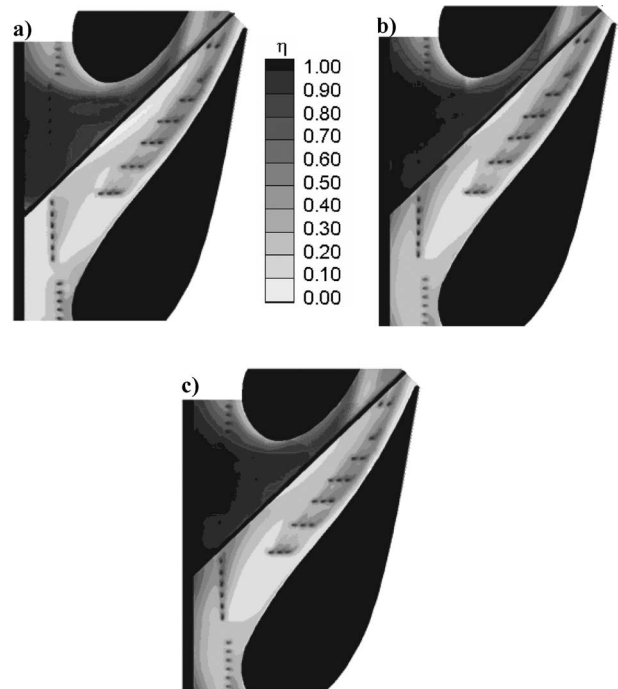


Fig. 13 Contours of adiabatic effectiveness on a rough endwall with cascade setting for different upstream slot flow rate with 0.5% film cooling: (a) 0.75% ($I=0.08$) slot flow; (b) 0.95% ($I=0.12$) slot flow; (c) 1.1% ($I=0.16$) slot flow

region is no longer present, which was shown at the 0.75% coolant flow condition about one-third of the way downstream of the midpassage slot. It is also interesting to note that the film-cooling holes on the pressure side of the midpassage gap showed better cooling as the slot flow was increased to 0.95% relative to 0.75%.

6 Conclusions

Measurements of endwall and midpassage gap adiabatic effectiveness were presented for an endwall surface with realistic features, namely a combustor-to-turbine interface gap, endwall film cooling, a vane-to-vane midpassage gap, a platform misalignment, and surface roughness. When compared to a smooth surface, it was observed that the effect of roughness could vary. For the higher blowing ratio, there was a definite decrease in adiabatic effectiveness due to roughness but, for the lower blowing ratio, there was essentially no difference in cooling. This difference was related to the boundary layer thickness, whereby a thicker boundary layer had a significant impact on the jet separation from the endwall in the case of a high blowing ratio.

The midpassage gap had a significant impact on the progression of the upstream coolant, whereby the gap limited the area of coverage for the upstream slot coolant flow. The cooling from the upstream slot had a beneficial effect only along the suction side surface of the vane. Measurements, along with an inviscid analysis, indicated that fluid from the platform was ingested into the midpassage gap. Near the start of the gap, most of the flow ingested was coolant, which rapidly decayed because of the hot gas ingested.

Platform misalignment proved to also have a substantial effect on endwall adiabatic effectiveness levels. Clearly, from a heat transfer standpoint, a cascade configuration would be the most desirable endwall alignment mode. The cascade setting showed considerably better adiabatic effectiveness levels relative to an aligned or dam endwall configuration, nearly removing the need for cooling holes on the suction side of the endwall. From a tur-

bine design standpoint, the cascade setting is ideal relative to a dam configuration, as the cascade acts like a trench where the coolant flow can reside.

This study has shown the drastic effects that realistic turbine features can have on first-stage nozzle platform cooling. Upstream slot flow and a cascade misalignment provide for better cooling on the endwall. Quite the opposite is the case for a misaligned dam, midpassage gap, and, in some cases, endwall surface roughness. These competing effects, when properly understood, can be used to better design endwall cooling arrangements.

Acknowledgment

This publication was prepared with the support of the U.S. Department of Energy, Office of Fossil Fuel, and National Energy Technology Laboratory. However, any opinions, findings, conclusions, or recommendations expressed herein are solely those of the authors and do not necessarily reflect the views of the DOE. The authors would also like to thank Mike Blair (Pratt & Whitney), Ron Bunker (General Electric), and John Weaver (Rolls-Royce) for their input on the modeling of realistic turbine features.

Nomenclature

C	= true chord of stator vane
C_a	= axial chord of stator vane
D	= diameter of film cooling hole
I	= momentum flux ratio
L	= length of midpassage gap
\dot{m}	= mass flow rate
M	= mass flux/blowing ratio
P	= vane pitch; hole pitch
P_o or p	= total and static pressures
Re_{in}	= Reynolds number defined as $Re = CU_\infty / \nu$
s	= distance along vane from flow stagnation
S	= span of stator vane
T	= temperature
x, y, z	= local coordinates
u, v, w	= local velocity components
U	= velocity global
W	= midpassage gap width

Greek Symbols

η	= adiabatic effectiveness, $\eta = (T_\infty - T_{aw}) / (T_\infty - T_c)$
ρ	= density
ν	= kinematic viscosity
θ	= nondimensionalized gap effectiveness, $\theta = (T_\infty - T_G) / (T_\infty - T_c)$

Subscripts

aw	= adiabatic wall
----	------------------

c	= coolant conditions
G	= gap
in	= inlet conditions
j	= coolant flow through film-cooling holes
s	= flow through upstream slot
∞	= free-stream conditions

References

- [1] Blair, M. F., 1974, "An Experimental Study of Heat Transfer and Film-cooling on Large-Scale Turbine Endwall," ASME J. Heat Transfer, **96**, pp. 524–529.
- [2] Burd, S. W., Satterness, C. J., and Simon, T. W., 2000, "Effects of Slot Bleed Injection Over a Contoured Endwall On Nozzle Guide Vane Cooling Performance: Part II—Thermal Measurements," ASME Paper No. 2000-GT-200.
- [3] Colban, W. F., Thole, K. A., and Zess, G., 2002, "Combustor-Turbine Interface Studies: Part 1: Endwall Measurements," ASME J. Turbomach., **125**, pp. 193–202.
- [4] Colban, W. F., Lethander, A. T., Thole, K. A., and Zess, G., 2002, "Combustor-Turbine Interface Studies: Part 2: Flow and Thermal Field Measurements," ASME J. Turbomach., **125**, pp. 203–209.
- [5] Friedrichs, S., Hodson, H. P., and Dawes, W. N., 1996, "Distribution of Film-Cooling Effectiveness on a Turbine Endwall Measured Using the Ammonia and Diazo Technique," ASME J. Turbomach., **118**, pp. 613–621.
- [6] Friedrichs, S., Hodson, H. P., and Dawes, W. N., 1997, "Aerodynamic Aspects of Endwall Film-Cooling," ASME J. Turbomach., **119**, pp. 786–793.
- [7] Friedrichs, S., Hodson, H. P., and Dawes, W. N., 1999, "The Design of an Improved Endwall Film-Cooling Configuration," ASME J. Turbomach., **121**, pp. 772–780.
- [8] Zhang, L. J., and Jaiswal, R. S., 2001, "Turbine Nozzle Endwall Film-cooling Study Using Pressure Sensitive Paint," ASME J. Turbomach., **123**, pp. 730–738.
- [9] Kost, F., and Nicklas, M., 2001, "Film-Cooled Turbine Endwall in a Transonic Flow Field: Part I—Aerodynamic Measurements," ASME Paper No. 2001-GT-0145.
- [10] Nicklas, M., 2001, "Film-Cooled Turbine Endwall in a Transonic Flow Field: Part II—Heat Transfer and Film-Cooling Effectiveness," ASME J. Turbomach., **123**, pp. 720–729.
- [11] Knost, D. G., and Thole, K. A., 2003, "Computational Predictions of Endwall Film-Cooling for a First Stage Vane," ASME Paper No. GT2003-38252.
- [12] Knost, D. G., and Thole, K. A., "Adiabatic Effectiveness Measurements of Endwall Film-Cooling for a First Stage Vane," ASME Paper No. GT2004-52236.
- [13] Yu, Y., and Chyu, M. K., 1998, "Influence of Gap Leakage Downstream of the Injection Holes on Film-cooling Performance," ASME J. Turbomach., **120**, pp. 541–548.
- [14] Aunapu, N. V., Volino, R. J., Flack, K. A., and Stoddard, R. M., 2000, "Secondary Flow Measurements in a Turbine Passage with Endwall Flow Modification," ASME J. Turbomach., **122**, pp. 651–658.
- [15] Ranson, W., Thole, K. A., and Cunha, F., 2004, "Adiabatic Effectiveness Measurements and Predictions of Leakage Flows Along a Blade Endwall," IMECE2004-62021.
- [16] Yamao, H., Aoki, K., Takeishi, K., and Takeda, K., 1987, "An Experimental Study for Endwall Cooling Design of Turbine Vanes," IGTC-1987, Tokyo, Japan.
- [17] Bons, J. P., Taylor, R. P., McClain, S. T., and Rivir, R. B., 2001, "The Many Faces of Turbine Surface Roughness," ASME Paper No. 2001-GT-0163.
- [18] Bogard, D. G., Schmidt, D. L., and Tabbita, M., 1998, "Characterization and Laboratory Simulation of Turbine Airfoil Surface Roughness and Associated Heat Transfer," ASME J. Turbomach., **120**, pp. 337–342.
- [19] Moffat, R. J., "Describing the Uncertainties in Experimental Results," Exp. Therm. Fluid Sci., **1**, pp. 3–17.